

# We are IntechOpen, the world's leading publisher of Open Access books Built by scientists, for scientists

6,900

Open access books available

186,000

International authors and editors

200M

Downloads

Our authors are among the

154

Countries delivered to

TOP 1%

most cited scientists

12.2%

Contributors from top 500 universities



WEB OF SCIENCE™

Selection of our books indexed in the Book Citation Index  
in Web of Science™ Core Collection (BKCI)

Interested in publishing with us?  
Contact [book.department@intechopen.com](mailto:book.department@intechopen.com)

Numbers displayed above are based on latest data collected.  
For more information visit [www.intechopen.com](http://www.intechopen.com)



---

# Structural and Dynamical Properties of Metallic Glassy Films

---

Hui Li, Weikang Wu and Kun Zhang

Additional information is available at the end of the chapter

<http://dx.doi.org/10.5772/64107>

---

## Abstract

In this chapter, a series of molecular dynamics simulations have been carried out to explore structural and dynamical features of monatomic liquid metallic films during rapid cooling. Results show a semi-ordered inhomogeneous morphology containing crystal-like and disordered regions. The icosahedron contributes to nucleation through the synergy with other short-range ordered structures and participates in crystal growth via assimilation, but the pinning effect should be overcome. The second-peak splitting in pair correlation functions is found as the result of a statistical average of crystal-like and disordered structural regions, not just the amorphous structure. The splitting can be viewed as a prototype of crystal-like peaks exhibiting distorted and vestigial features. Besides, we use the parameter  $P(a, \tau, \nu)$  for predicting both local structural order and motion propensity. The fraction of crystalline clusters follows a negative power-law scaling with the cooling rate increasing, which is the inverse of  $P(a, \tau, \nu)$ .

**Keywords:** molecular dynamics simulation, metallic glass film, structural evolution, dynamical feature, pair correlation function, local icosahedral order

---

## 1. Introduction

Ultrathin metallic glassy films with a thickness of one or a few monolayers attract much attention, since they are now available as epitaxial films on insulating substrates and are, therefore, the best model systems for two-dimensional (2D) conduction in metal systems [1]. Disorder is known to play an important role in the phase diagram of the superconductor material at low temperatures and high magnetic fields [2]. Significant effort is currently being invested in attempting to understand theoretically the interplay between disorder and the conductivity in 2D sys-

tems [3–5]. Specifically, in semiconductor field, thinner and thinner disordered films are needed, since the restriction to a thickness of a few monolayers may lead to novel atomic structures and modify the physical and chemical properties dramatically [6–8]. Huang et al. [9] reported the accidental discovery of 2D amorphous silica supported on grapheme. They found that the images of 2D amorphous silica contain both the crystalline and amorphous regions. Lichtenstein et al. [10] studied the interface between a crystalline and amorphous phase of silica film supported by the Ru(0001) substrate. The atomic structure of the topological transition from a crystalline to an amorphous phase in the thin silica film can lead to a better description of the crystal-to-glass and the liquid-to-glass transitions. Although there has been much progress in the understanding of the properties of amorphous materials in three-dimension [11–13], some important questions on the microstructural feature and its forming mechanism of the metallic glassy films have remained unanswered. Therefore, further studies on the atomic structures of the 2D disordered systems and their physical proprieties are necessary [14–16].

This chapter is organized as follows. In Section 2, we describe the modeling and simulation methods. In Section 3, we discuss the structural evolution of liquid metallic nano-film during rapid solidification as well as the effect of cooling rates [17, 18]. In Section 4, we consider the motion propensity distribution to predict both local structural distribution and dynamical signature in metallic nano-films [18]. In Section 5, we study the synergy and pinning effects of the local icosahedral order during freezing [17]. In Section 6, we clarify the origin of the splitting of the second peak in PCFs based on a statistical explanation [19]. Conclusions are provided in Section 7.

## 2. Models and theoretical methods

Molecular dynamics (MD) simulations were performed using the embedded atom method (EAM) potential [20] supplied in LAMMPS [21]. The pure copper film and the pure cobalt film are studied respectively. For the copper film, 6400 copper atoms were distributed in a  $20 \times 20 \times 1$  lattice unit box based on the structure of FCC crystal and the initial box lattice was set to be 3.61 Å. For the cobalt film, the initial configuration consisting of 8640 cobalt atoms was distributed in a  $60 \times 36 \times 1$  lattice unit box, in which atoms were arranged in the light of the HCP crystal structure and the box lattice was set to 2.507 Å. Periodic control was exerted on the  $x$ - and  $y$ -directions of the box, and the  $z$ -direction was nonperiodic. Specially, the lower boundary of the simulation box along the  $z$ -direction (not refer to atoms) was fixed, while the upper boundary was free. That was to say, a virtual wall was set at the lower edge of the simulation box in the  $z$ -direction, which is similar to the substrate in experiment.

The Velocity-Verlet algorithm was used with an MD time step of 1 fs while the temperature was controlled by a Nosé-Hoover thermostat [22]. A well-equilibrated initial system was prepared by gradually heating perfect crystals to melt at a low heating rate and then relaxing the system at 2000 K for 500 ps. Then, the liquid system was quenched to 300 K at different cooling rates. At each cooling rate, the atomic configuration during the quenching process were recorded for further analysis.

### 3. Structural features in liquid metallic nano-films during rapid cooling

**Figure 1** shows the potential energy landscape of the liquid copper nano-film at the temperature of 2000 K, which is composed of single-string structures and partial ring structures (we find the ring structure is the icosahedron). We call the icosahedron in our simulations the quasi-two-dimensional icosahedron (Q2D-I) because of one missing vertex atom due to the dimensional limit. Atoms in single-string structures show high potential energy and motion propensity, while Q2D-Is have a high dense packing [23]. Actually, in the melt film, both structures disintegrate and reunite frequently owing to the random collision and energy transfer of high-energy atoms. Besides, ensembles of atoms in different regions of this liquid film exhibit temporarily enhanced or diminished mobility in comparison with the average. Notably, the cooperative motion of single-string structures is dominant in the metallic liquid film, in accordance with that in three-dimensional liquids [23–25].

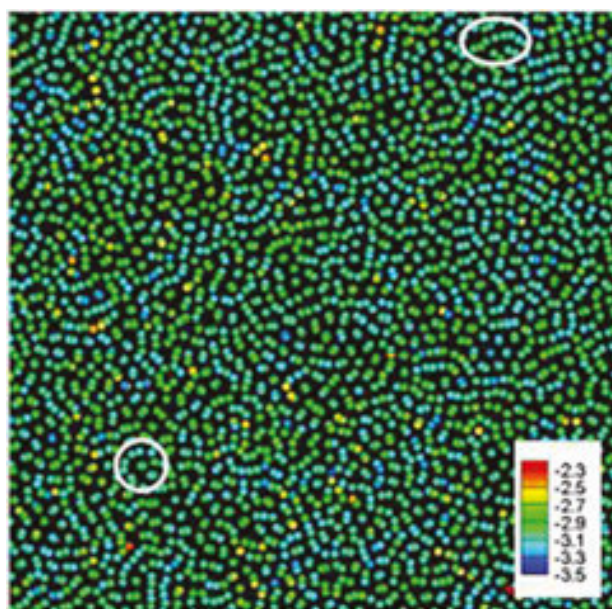


**Figure 1.** The potential energy landscape of the copper nano-film at 2000 K. The denoted circular region represent the quasi-two-dimensional icosahedron (Q2D-I) and the elliptical one represents the single-string structure.

As the temperature decreases, atoms in the 2D liquid copper tend to gather into clusters. To clarify the liquid-solid transition mechanism in metallic films during the cooling process in the view of an atomic level, the structural evolutions at different cooling rates are investigated as shown in **Figure 2**. At high cooling rates (250 and 500 K/ps), a semi-ordered morphology exhibiting maze-like nano-patterns gradually forms at 300 K. To be specific, at 500 K/ps, compared with the atomic configuration at 2000 K (**Figure 1**), Q2D-Is increases obviously accompanying with the decrease of single-string structures at 1200 K. When the temperature decreases into 900 K, Q2D-Is show continuous increase while the single-string structures begin to arrange side by side, forming crystalline zones. The size scale of crystalline zones in the

simulation is beyond 10–20 Å, meeting the size requirement of MRO (5–20 Å [26]). Thus, the crystalline zone can be considered as the MRO. Notably, these MRO structures are the precursor for nucleuses, whereas Q2D-Is would have barrier effects on nucleation. During the rapid cooling process, Q2D-Is and crystalline zones compete against each other and finally determine the solid structure at 300 K. For example, at 500 K/ps, Q2D-Is play the leading role since crystalline zones are limited due to the high cooling rate, and the system exhibits the most disorder at 300 K. However, when the lower cooling rate (250 K/ps) is performed, crystalline zones tend to be dominant, and finally the film system shows more crystalline MRO characteristics. Although the crystalline MRO gradually forms and develops during rapid cooling, the transition time is so transient that crystalline zones cannot be converted into the crystalline long-range order (CLRO). In contrast, in the case of 10 K/ps (as shown in **Figures 2g–i**), owing to the absence of the icosahedral frustration effect, atoms are mainly arranged in an crystalline order.

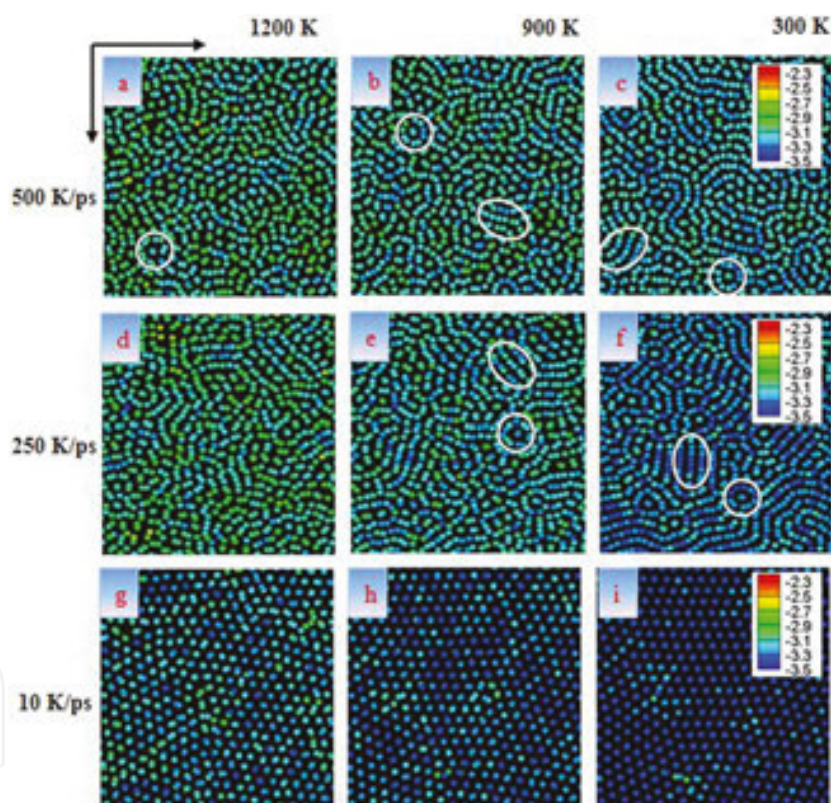


**Figure 2.** Quenching processes at different temperatures with three different cooling rates. The denoted circular region represent the Q2D-I and the elliptical one represents the crystalline zone.

To further investigate the influence of the cooling rate on the phase transition of metallic films, both the pair correlation functions (PCFs) and the proportion of crystalline zones at different cooling rates are plotted. The crystallization moments can be characterized by the pressure drops [27], indicating a linear relation between the crystallization moment and the supercooled melt lifetime. However, the faction of crystalline zones in this simulation is determined

through the statistical average of the recorded structural information [28, 29], which is different from Morozov et al.'s method [27]. As shown in **Figure 3a**, the highest cooling rate (500 K/ps) leads to a slight splitting second peak in the PCF curve, while at 250 K/ps, the second peak exhibits obvious splitting and a small shoulder peak appears between the first peak and the second peak. Although the second peak splitting of the PCF curve is usually considered as an important signature of amorphous solids [30], we would rather regard it as the formation of crystalline zones which can be seen as a precursor to the CLRO [31]. At a low cooling rate, such as 10 K/ps, the PCF curve presents typical crystalline features: the splitting characteristic of the PCF second peak becomes more obvious; the small shoulder peak changes into a sharper peak. During the slow cooling process, Q2D-Is disappear while the crystalline MRO integrates together, leading to the CLRO characteristic of the metallic film. **Figure 3b** shows the crystalline fraction change of the above three queching processes. At the high cooling rate (500 and 250 K/ps), the FCC and HCP structures exhibits a similar amount and shows little changes during the cooling process. However, at 10 K/ps, both the FCC structure and the HCP structure grow fast between 800 and 500 K, and finally FCC structures become the dominant with the faction of more than 50% at 300 K. Such results strongly indicate a non-linear relation between the crystallization fraction and the freezing time, quite different from the Morozov's result in bulk liquid metals [27].

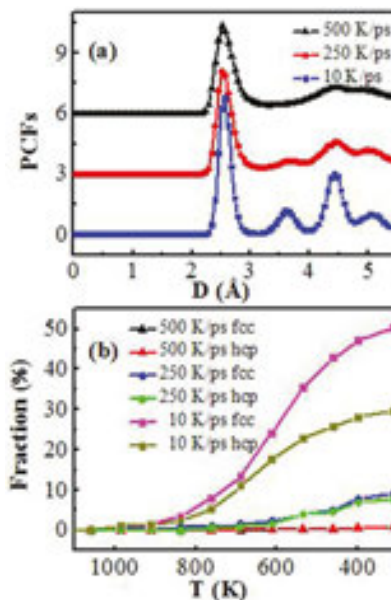


**Figure 3.** (a) Pair correlation functions (PCFs) at 300 K; (d) the fraction of crystalline zones during the cooling processes.

#### 4. Power-law scaling of dynamical signatures

In this section, the motion propensity distribution is considered to predict the structural and dynamical features of the liquid copper nano-film. First, the Common Neighbor Analysis

(CNA) and motion propensity are introduced to reveal the relation between crystalline MRO and the subsequent crystallization. The CNA can be used to measure the local crystalline structure around an atom [28, 29, 32], based on the Honeycutt and Andersen bond analysis [33]. Generally, there are five kinds of CNA patterns that LAMMPS recognizes, which are defined as follows: FCC = 1, HCP = 2, BCC = 3, icosahedral = 4, and unknown = 5. The first three indices are all “crystalline”. Also note that the CNA calculation in LAMMPS uses the neighbors of an owned atom to find the nearest neighbors of a ghost atom. The local motion propensity of a particle [34, 35] is directly associated with the probability of a particle undergoing a substantial displacement within a short time interval. The motion propensity of a particle  $p$  is defined as follows:

$$Q_t(a, \tau, v) = \frac{1}{N} \sum_p \exp \left( - \frac{\|\Delta \vec{r}_p(t, t+\tau)\|^2}{2a^2} \right), \quad (1)$$

where  $\|\Delta \vec{r}_p(t, t+\tau)\|$  is the displacement of the particle  $p$  obtained from the quenched configuration between  $t$  and  $t + \tau$  and  $a$  is the length scale over which the motion is probed. Here  $a = 0.29$ , and  $\tau = 1000$  fs [36].

**Figure 4** shows the CNA pattern and the motion propensity distribution of quenched films at different cooling rates. When the cooling rate is high (500 K/ps), although the barrier effect of Q2D-Is is prominent, several ordered crystalline clusters, such as FCC and HCP structures, still exist at 300 K, indicating that the so-called “full amorphous state” may contain few crystalline SRO structures, namely the crystallite. However, due to the limitation of experimental methods, it is hard to measure the real atomic arrangement within the SRO range. Actually, these crystallites are quite stable, which can be seen from their motion propensity distribution as shown in **Figure 4a**. As the cooling rate reduce, it can be clearly seen that crystallites are rare and discrete initially, but appear at random positions, exhibiting a large structural heterogeneity of the metallic glassy film [37]. At 250 K/ps, more crystallites appear and grow in size at 300 K as shown in **Figure 4b**. A two-step crystallization process is proposed [38]: first, the fluctuations of structure and energy cause the formation of several SRO crystallites which can precursors for the nucleus of crystalline zones; Then, the crystallites expand into surrounding and form crystalline zones. Notably, the FCC or HCP structures do not emerge alone. Instead, the crystalline zone is made up of alternant FCC and HCP structures as presented in the CNA patterns. When the cooling rate is quite low, there would be enough relaxation time for the evolution from HCP structures to FCC structures, similar to Wolde et al.'s viewpoint [39]. For example, at 10 K/ps, the weakening barrier effect of Q2D-Is would result in the ordered atomic arrangement and the formation of nano-polycrystalline structures dominated by FCC structures at 300 K. The appearance of HCP structures is actually just an intermediate state during the crystallization. Besides, it is worth noting that, the complete-disorder region is characterized by high motion propensity, whereas the low motion propensity is related to the crystalline zones. Generally, the basic principle of local propensity  $Q_t(a, \tau,$

$v$ ) is that the configurational order does not determine the motion of a neighborhood directly but affects the probability of the undergoing motion. Therefore, a theoretical discussion is necessary to verify the possible relation between the structure and dynamics.

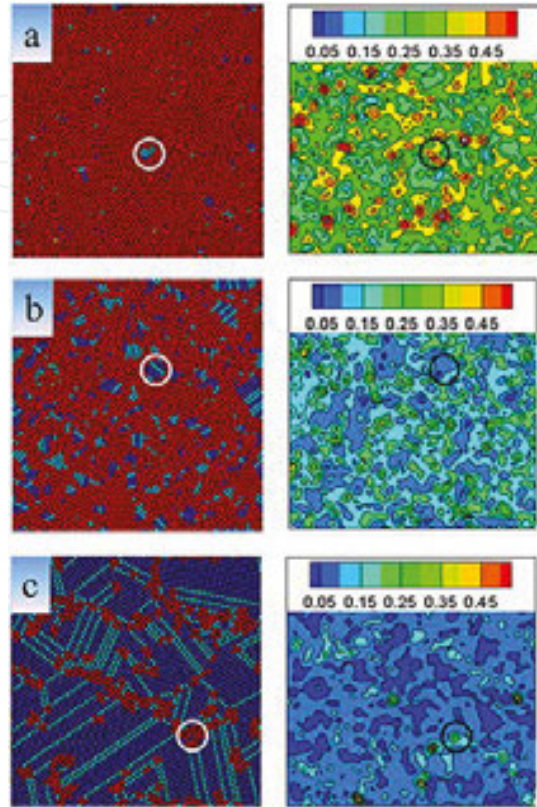


**Figure 4.** Local atomic ordering (left) and motion propensity (right) of the quenched structures at 300 K with different cooling rates: (a) 500 K/ps; (b) 250 K/ps; (c) 10 K/ps. In the left column, local structures are colored based on the CNA method: blue, FCC; green, HCP; red, disordered structures. In the right column, coloring denotes the motion propensity.

Next, we emphatically studied the relation between the total motion propensity and the crystalline-like structure in the copper film at different cooling rates.  $Q_{sd}$  is the standard deviation of the total motion propensity obtained from the quenched configuration at 300 K during a short relaxation time, which may reflect the total fluctuation of the 2D system with respect to time clearly. **Figure 5a** shows the  $Q_{sd}$  change as a function of time during a short period  $\phi = 1000$  fs, at different cooling rates. For the quenched structure under the highest cooling rates, its  $Q_{sd}$  shows the highest dynamical fluctuation during the relaxation, indicating that the system is in the metastable state. In contrast, the dynamical fluctuation at a lower cooling rate exhibits less obvious features, in good accordance with **Figure 4**. This means that the total motion propensity is reliable to measure the system stability. For further exploration, a global measure of the propensity  $P(a, \tau, v)$  is calculated by the correlation function  $Q_i(a, \tau, v)$ :

$$P(a, \tau, v) = N \sum_p [Q_i(a, \tau, v) - 1]^2. \quad (2)$$

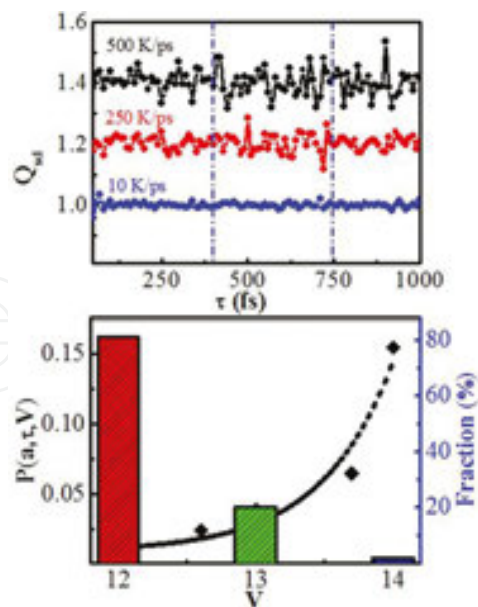


**Figure 5.** (a) The standard deviation ( $Q_{sd}$ ) of the total motion propensity and (b) the relationship between the total motion propensity (left) and the fraction of crystalline zones (right) at different cooling rates.

where  $v = \log V$ ,  $V$  is the cooling rate.  $Q_i(a, \tau, v)$  is the motion propensity of a single particle.

**Figure 5b** shows the relationship between  $P(a, \tau, v)$  and the crystalline fraction at 300 K, with respect to the cooling rate. As the cooling rate increases, the fraction of crystalline zones increases and shows an index relationship with the cooling rate. For a low cooling rate ( $v < 12.5$ ), the copper film exhibits a dominant crystalline characteristic with a relatively low  $P(a, \tau, v)$  ( $P < 0.025$ ). However, when the cooling rate increases ( $v > 13.8$ ), Q2D-Is in the metallic film become dominant leading to a high value of  $P(a, \tau, v)$  ( $P > 0.075$ ). At a moderate cooling rate, such as  $v = 13.8$ , a complicated amorphous-crystalline composite forms, with the FCC and HCP structures distributing randomly and exhibiting the crystalline MRO characteristic. Obviously, the fraction of crystalline zones exhibits a negative power-law scaling with the cooling rate, which is the inverse of  $P(a, \tau, v)$ . This indicates a close relationship between  $P(a, \tau, v)$  and the crystalline structure as the cooling rate increases. Such phenomena have not been reported in experimental research, due to some factors associated with multiple scattering and the atomic cluster distortion. To conclude, as a new parameter,  $P(a, \tau, v)$  may be a direct consequence of the local structural ordering and the dynamic signature may also result from the local structural ordering.

## 5. Synergy and pinning effects of local icosahedral order

The above results show that, Q2D-Is appear earlier than crystalline zones during the cooling and can be preserved under the higher cooling rate since the local icosahedral order (LIO) grows with severe undercooling [40]. When crystalline zones emerge, the quantity of Q2D-Is decreases, indicating that Q2D-Is influence the formation of the CMRO.

**Figure 6a** shows how crystalline zones nucleate through the synergy effect of Q2D-Is. It should be pointed out that, the single-string structure is the basic unit of crystalline zones since it can extend to form the close-packed plane (CPP), similar to the expansion of a graphene piece into a graphite layer. **Figure 6d** reveals the similar topological unit between Q2D-Is and CPPs, which is the structural basis for the assimilation of Q2D-Is. Initially, in the supercooled melt, owing to the strong atomic activity, the SRO structures including the single-string structure and Q2D-Is disintegrate and reunite frequently. During the nucleation, several Q2D-Is are decomposed and integrate into the nucleus with the help of single-string structures, indicating that the LIO should be the raw component of the crystal nucleus. **Figures 6b, c** show the growth of crystalline zones with the assistance of Q2D-Is in the parallel and perpendicular direction to CPPs, respectively. In the parallel growth, when Q2D-Is are contacted by the front of crystalline zones, Q2D-Is would be touched by the CPPs naturally due to their similar topological unit, leading to the gradual assimilation (see **Figure 7** in detail). On the other hand, when the crystalline zones grow in the perpendicular direction and contact a Q2D-I, a suitable connection to the Q2D-I by the surrounding single-string structures or CPPs would assimilate the Q2D-I into the crystalline structures, leading to the perpendicular growth of crystalline zones. Thus, Q2D-Is show the synergy effect during the whole crystallization process. Notably, icosahedra are usually seen as a barrier to crystallization [40], but these results demonstrate that icosahedra can participate the crystal growth through the synergy effect in the 2D system, providing a new view of the correlation between the LIO and crystallization.

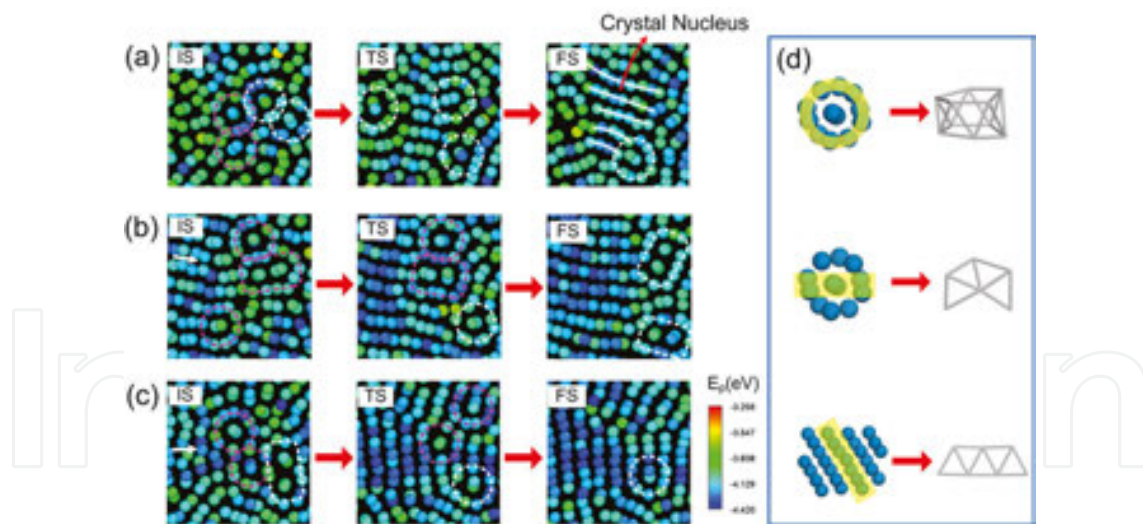


**Figure 6.** (a) A crystal nucleus forms through the synergy between Q2D-Is and single-string structures. The crystal nucleus is characterized by white solid lines. (b, c) crystalline zones grow through through the assimilation of Q2D-Is in the direction parallel and perpendicular to the close-packed planes (CPPs), respectively. The Q2D-Is are characterized by dotted circles and rounded rectangles. The IS, TS and FS represent the initial state, transition state and final state, respectively. (d) Q2D-Is and CPPs have the similar topological unit. From top to bottom: the side structure of Q2D-Is, longitudinal section of Q2D-Is and CPP.

Next, the detailed assimilation of Q2D-Is by crystalline zones is investigated to explore the mechanism of the synergy effect. **Figure 7a** shows the assimilation process of a Q2D-I by

crystalline zones in the direction parallel to CPPs. The contact between CPPs of crystalline zones and a Q2D-I would result in a half-icosahedral and half-crystalline geometrical frustration, as illustrated in **Figure 7b**. Then, the Q2D-I is gradually assimilated as the geometrical frustration evolves into the crystalline order. According to **Figure 7c**, during the assimilation, the Q2D-I experiences an energy fluctuation accompanying with an obvious oscillation for the average potential energy. In order to measure the energy fluctuation, the root mean squared deviations (RMSDs) [41] are calculated based on the mean value of energy fluctuations in the whole system:  $\text{RMSD} = \sqrt{\frac{1}{N} \sum_{i=1}^N |\Delta E_i - \overline{\Delta E}|^2}$ , where  $N$  is the atomic number,  $\Delta E_i$  is the potential energy fluctuation per atom,  $\overline{\Delta E}$  is the average of  $\Delta E_i$ . The average fluctuation of the system during the process in **Figure 7** is  $0.04347915 \pm 0.02080011$  eV (where,  $\overline{\Delta E} = 0.04347915$  eV and  $\text{RMSD} = 0.02080011$  eV). The fluctuation of Q2D-I just in the range indicates that energy fluctuations lead to the assimilation during the parallel growth. Thus, the Q2D-I can be actually seen as a pin during the assimilation, which needs to be drawn out for the growth of crystalline zones. In another word, Q2D-Is have pinning effects on the crystal growth due to the energy fluctuation. If the pinning effect can be overcome, the assimilation of Q2D-Is would assist the growth of crystalline zones, presenting the synergy effect of the LIO.

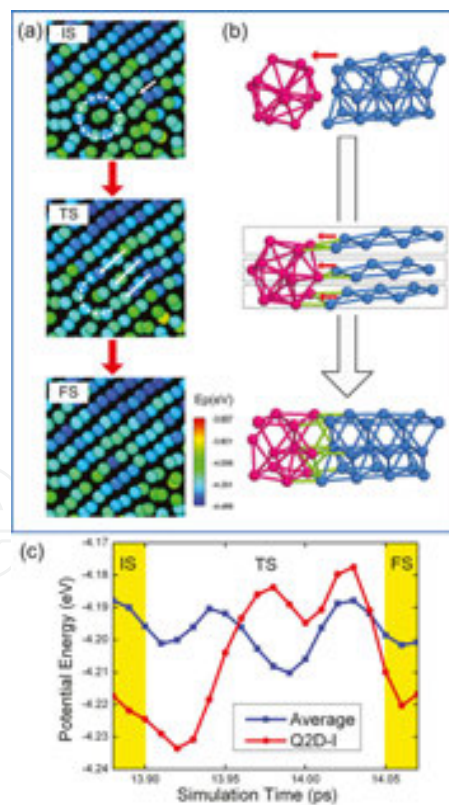


**Figure 7.** (a) A Q2D-I is assimilated by crystalline zones in the direction parallel to CPPs. White solid arrows show the crystal growth direction. (b) Detailed structural evolution during the assimilation. Three adjacent CPPs naturally connect to the Q2D-I with red solid arrows showing the direction. (c) Potential energy change during the assimilation. The curve of the Q2D-I shows potential energy fluctuations during the assimilation.

**Figure 8** shows that the crystalline zone assimilates a Q2D-I in the direction perpendicular to CPPs, which presents more complicated features than that in the parallel growth. However, under closer observation, the assimilation process is very similar to that during a parallel growth. When crystalline zones touch a Q2D-I, the Q2D-I would be gradually connected by the surrounding CPPs, revealing that the crystal growth in the direction perpendicular to CPPs originate from the connection between CPPs and Q2D-Is in the parallel direction. **Figure 8b** presents that the Q2D-I also undergoes a potential energy fluctuation and the average energy oscillates during the assimilation. The potential energy fluctuations during the perpendicular growth indicate the pinning effect of Q2D-Is. The average fluctuation of system is  $0.04774295 \pm 0.01739893$  eV (where,  $\Delta E = 0.04774295$  eV and  $RMSD = 0.01739893$  eV), and the Q2D-I's energy fluctuation leads to the leap over the pinning effect during the perpendicular growth. Once the pinning effect succeeds, Q2D-Is might survive as shown in **Figure 9**. In this case, the surrounding CPPs have to bend to cater to the Q2D-I due to the incompatibility between Q2D-Is and the crystals, exhibiting the geometrical frustration. In another word, the Q2D-I is actually a pin, causing the geometrical frustration of the surrounding crystalline order.

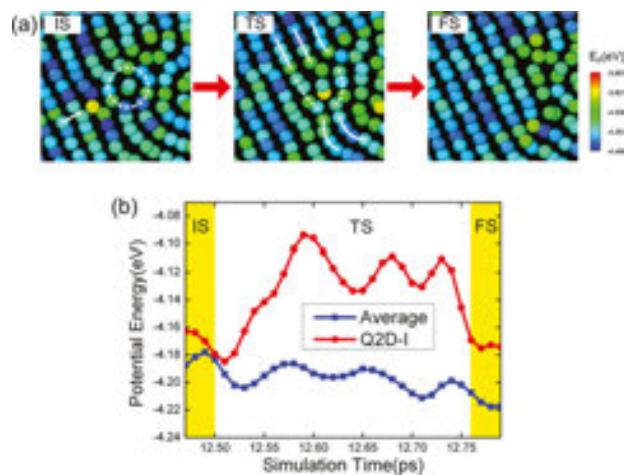


**Figure 8.** (a) A Q2D-Is is assimilated by crystalline zones in the direction perpendicular to CPPs. White solid arrows show the crystal growth direction. The assimilation in (a) is very similar to that in the parallel growth. (b) Potential energy change during the assimilation. The curve of the Q2D-I shows potential energy fluctuations during the assimilation.

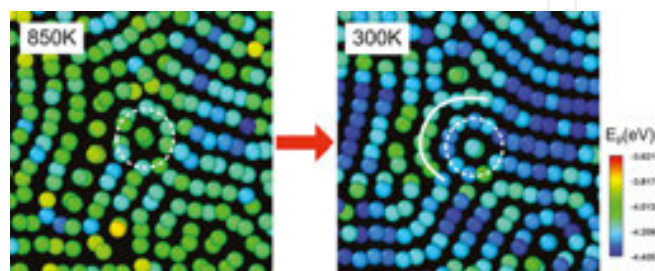


**Figure 9.** Preservation of a Q2D-I due to the pinning effect. The solid arc line shows the frustrated CPP catering to the Q2D-I.

## 6. Origin of the second peak splitting in pair correlation functions

A splitting of the second peak in the PCF curve in three-dimensional materials is usually regarded as a characteristic indication of disordered structure forming [42, 43]. However, owing to the lack of one dimensionality as well as the difference of atomic arrangement, the explanation on the second peak of the PCF in 2D systems should be clarified. In addition, previous studies are usually based on the viewpoint of how the clusters connect to each other to form a large supercluster with a specific geometric structure. Due to the fact that the PCF is the statistical average of the atomic configuration, it seems more appropriate to use the statistical methods to interpret the nature of the second peak splitting of the PCF in 2D system. Actually, fewer efforts have focused on the relation between the splitting of the second peak and the crystalline or glass formation of 2D disordered films by statistical average analysis. In order to understand these questions well, this section would provide a statistical explanation on the nature of the splitting of the PCF in the 2D copper system.

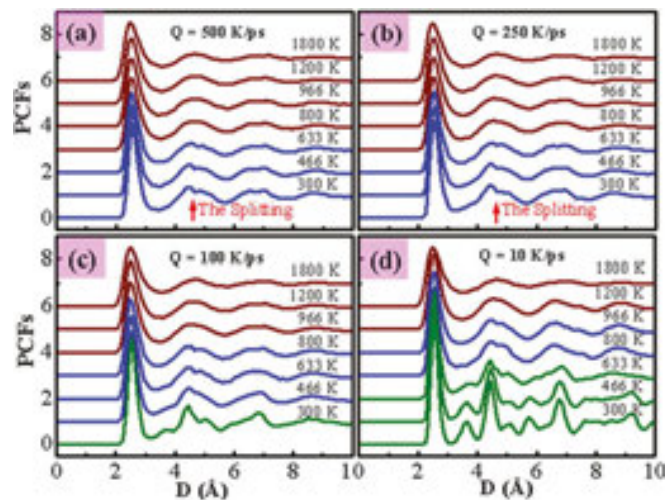


**Figure 10.** PCF evolutions of the 2D copper at different cooling rates: (a) 500 K/ps; (b) 250 K/ps; (c) 100 K/ps; (d) 10 K/ps. Brown curves represent the PCF without the second peak splitting; Blue curves show the second peak splitting; Green curves show typical crystal peaks.

The PCFs of the 2D copper are shown in **Figure 10**. It is worth noting that the main peak height of the PCFs, which represents the nearest-neighbor shell, increases significantly with the decreasing temperature, and the second peak begins to split. As shown in **Figures 10a, b**, at the cooling rates of  $Q_1 = 100$  K/ps and  $Q_2 = 250$  K/ps, the second peak begins to split into two subpeaks at 633 K. Interestingly, a small shoulder peak appears between the first and second peaks at 300 K in **Figure 10b**, which means the short- or medium-range ordered structures form. With the cooling rate decreasing to  $Q_3 = 100$  K/ps, the splitting emerges at 800 K; moreover, the small shoulder peak between the first and second peaks arises on the left at 300 K with significant height, which indicates that the length of the ordered structure is further extended to a large scale. At the cooling rate of  $Q_4 = 10$  K/ps, the left shoulder peak arises at 633 K and becomes more prominent than the right subpeak as the temperature decreases,

suggesting that the orientation of the crystalline structure becomes more consistent. It is widely known that the atomic structure of amorphous materials is similar to that of liquid metals, and the fact that the second peak of the PCFs splits into two subpeaks is regarded as a characteristic indication of disordered structures. However, this is not the true case in 2D systems. As shown in **Figures 10c, d**, the evolution of the PCFs clearly indicates how the second-peak splitting converts into crystal peaks. For example, as shown in **Figure 10d**, at 800 K, the splitting of the second peak of the PCF appears, but at 633 K, the splitting of the second peak becomes three peaks, and finally these three peaks evolve into three typical crystal peaks at 466 K. Based on this evolution trend, it can be seen that the splitting second-peak has a close relationship with crystal peak, and that the splitting second-peak is the rudiment of the crystal peaks. Our simulations do not support other hypothesis which states that the splitting of the second peak occurs as a result of the connection of some small clusters to a supercluster with a special geometrical structure.

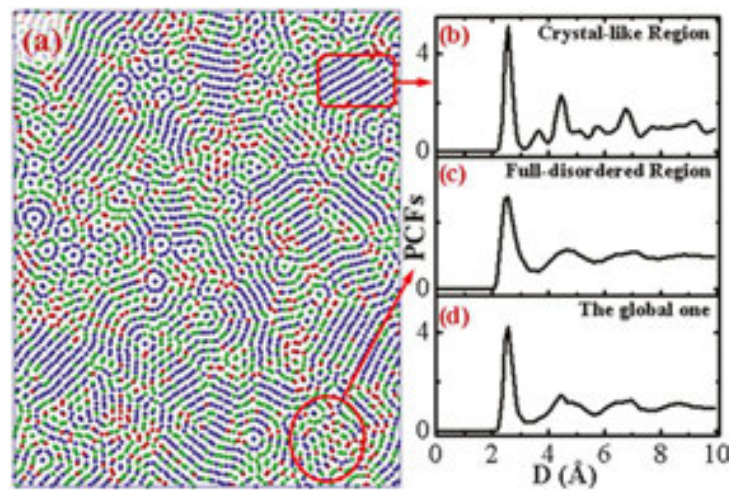


**Figure 11.** (a) Snapshot of the 2D copper at 300 K with the cooling rate of 250 K/ps. Crystal-like ordering regions are constituted by blue atoms, while other regions show fully disordered ordering. (b–d) PCF curves of different regions: local crystal-like regions, fully disordered regions, the global region, respectively.

In order to further clarify the origin of the splitting of the second peak, the structural configuration of the 2D copper at 300 K at the cooling rate of  $Q_2 = 250$  K/ps is supplied in **Figure 11**. It is seen that the overall atomic structure consists of two types of regions: the well-organized region with crystal-like order and the fully disordered region with some packing frustration. Our theoretical results are in good agreement with the experiments by Huang and Lichtenstein [9, 10], which prove our MD simulation result is reliable. It is also worth noting that in the disordered region there are some single strings, arcs, and rings which clearly illustrate the packing frustration of the atoms in the quick cooling process. In fact, **Figure 11a** shows that the structure of the 2D amorphous Cu is the mixture of crystal-like and fully disordered structural regions with a certain percentage. The local PCFs in these two distinct regions differ from one another. As shown in **Figures 10b–d**, the local PCFs of the crystalline region have some crystal-like subpeaks, showing typical crystalline features, while the local PCFs in the fully disordered structural region show no splitting on the second peak. However, the global

PCFs averaged by the overall atomic structures of the two types of regions show a slight splitting in the second peak. It is known that the PCF is the statistical average of the structural configuration, thus, the slight splitting of the global PCF is caused by the combined average results of the crystal-like and fully disordered regions. Moreover, the very similar results are also obtained for the simulations of the 2D cobalt, which indicate the coexistence of crystal-like and fully disordered regions. The splitting of the second peak in 2D systems may not be the signature of the glass formation, but the appearance of both the crystal-like and disordered structures. The splitting second-peak can be viewed as an embryonic form of the crystal peak.

The above results arouse us to further investigate the origin of these two subpeaks in the second-peak splitting. **Figure 12** shows the respective PCF curves of the liquid, amorphous, and ideal crystalline solid Cu. It is known that in ideal FCC crystal there are four nearest coordinated shells, namely,  $R_1 = 2.55 \text{ \AA}$ ,  $R_2 = 3.61 \text{ \AA}$ ,  $R_3 = 4.44 \text{ \AA}$ , and  $R_4 = 5.12 \text{ \AA}$ . The positions of the first peak in both the liquid and amorphous Cu correspond to the ones in the ideal FCC crystal at  $R_1 = 2.55 \text{ \AA}$ , while the second peaks correspond to three peaks of the ideal FCC crystal at the locations  $R_2 = 3.61 \text{ \AA}$ ,  $R_3 = 4.44 \text{ \AA}$ , and  $R_4 = 5.12 \text{ \AA}$ . From the correspondence of the peak positions and the evolution trend, it is concluded that the two subpeaks on the second peak are due to the appearance of a small amount of the short- or medium-range ordered structures.

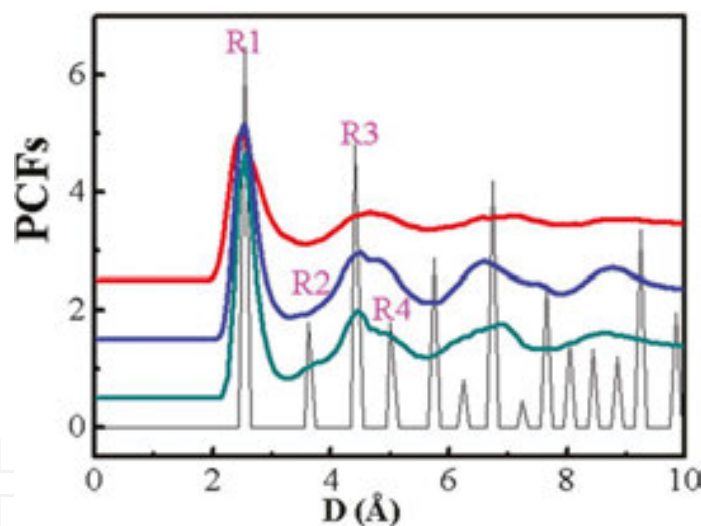


**Figure 12.** PCF curves of the liquid, amorphous, and ideal crystal copper. Red line: liquid at 1800 K; Blue line: amorphous solid at 300 K ( $Q = 400 \text{ K/ps}$ ); Green line: amorphous solid at 300 K ( $Q = 200 \text{ K/ps}$ ); Black line: ideal crystal.  $R_1$ ,  $R_2$ ,  $R_3$ , and  $R_4$  represent the ideal FCC peaks.

**Figure 13** shows the fraction of the crystal-like regions with the temperature at different cooling rates. If the splitting occurs on the right without the left subpeak, this point is labelled with a blue arrow, while if both the left and right subpeaks appear, it is labelled with a red arrow. According to this rule, **Figure 13** may be divided into three zones. When the fraction of the crystal-like region is less than 18.5%, it belongs to the non-splitting region corresponding to the fully disordered structure in the liquid state. If the fraction of crystal-like region exceeds to 50%, the left shoulder subpeak appears, which indicates it almost becomes the polycrystal-

line structure. However, if the fraction ranges from 18.5 to 50%, it is the mixture of the disordered and crystal-like structural regions, which results in the splitting second peak of the PCF. The disordered structure in 2D may be a simple mixture of crystal-like and fully disordered region, which sheds a new light on the understanding of the atomic structure of the low-dimensional materials.

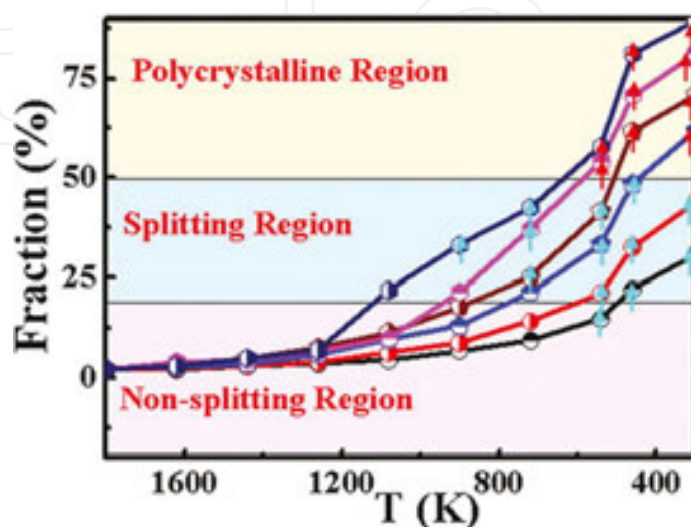


**Figure 13.** Relationship between the fraction of crystal-like regions and the second peak splitting at different cooling rates: 500 K/ps (blue line), 250 K/ps (red line), 100 K/ps (blue line), 50 K/ps (brown line), 25 K/ps (purple line), 10 K/ps (dark blue line).

## 7. Conclusion

In summary, we systematically investigate the structural evolution and dynamical properties of glassy metallic films during rapid cooling. Our results have shown several aspects as follows:

- A semi-ordered amorphous morphology with maze-like nano-patterns emerges as the temperature decreases at a high cooling rate. The growth competition between two typical dominating structures, Q2D-Is and crystalline zones, significantly affects the final solid-state structure. The FCC and HCP structures are alternant in the crystalline zone region, acting as the precursor of CLRO structures.
- The disordered region usually has a high motion propensity distribution, whereas a lower motion propensity corresponds to the crystalline-like order region. Both the local structural distribution and the dynamical signature in metallic nano-films can be predicted by an excellent indicator  $P(a, \tau, \nu)$ . The region with a lower  $P(a, \tau, \nu)$  can accommodate a larger crystallin-like order, and vice versa.
- The LIO has synergy and pinning effects on the freezing behavior of a monatomic liquid film. crystalline zones would gradually form through the synergy of Q2D-Is with other SRO

structures, but the pinning effect should be overcome when crystals grow in both the directions parallel and perpendicular to close-packed planes, consuming energy.

- The origin of the splitting of the second peak in PCFs is a statistical result of the disordered and crystal-like ordered structure with a certain percentage rather than the fully disordered structure. The results show that the shoulder peak on the left side of the second peak is due to the appearance of a small amount of the short-or medium- range ordered structures. The structure in 2D disordered film may be a simple mixture of the crystal-like and disordered structural regions.

## Acknowledgements

We would like to acknowledge the support by the national funds from Chinese government (Nos. 50971081, 50831003, 51271100 and No. 20090131110025). This work is also funded by the National Basic Research Program of China (Grant No. 2012CB825702). This work is also funded by the grants from Shandong Province in China (Nos. 50625101, JQ200817, and ZR2009FM043). This work is also supported by the Special Funding in the Project of the Taishan Scholar Construction Engineering. We also thank the support from Shandong University (No. 2009JQ014 and No. 31370070614018) and Shandong excellent young scientist science foundation BS2010CL027.

## Author details

Hui Li\*, Weikang Wu and Kun Zhang

\*Address all correspondence to: Lihuilmy@hotmail.com

KeyLaboratory for Liquid-Solid Structural Evolution and Processing of Materials, Ministry of Education, Shandong University, Jinan, People's Republic of China

## References

- [1] Pfennigstorf O., Petkova A., Guenter H.L., Henzler M. Conduction mechanism in ultrathin metallic films. *Physical Review B*. 2002;65(4):045412.
- [2] Wilkin N.K., Jensen H.J. Disorder driven destruction of a phase transition in the vortex system of a superconductor. *Physical Review Letters*. 1997;79(21):4254.
- [3] Crauste O., Couedo F., Bergé L., Marrache C., Dumoulin L. Superconductor-insulator transition in amorphous  $\text{Nb}_x\text{Si}_{1-x}$  thin films. comparison between thickness, density

- of state and microscopic disorder. In: *Journal of Physics: Conference Series*; IOP Publishing; 2012. p. 022012.
- [4] Strongin M., Thompson R.S., Kammerer O.F., Crow J.E. Destruction of superconductivity in disordered near-monolayer films. *Physical Review B*. 1970;1(3):1078.
- [5] Ulman A. Formation and structure of self-assembled monolayers. *Chemical Reviews*. 1996;96(4):1533–1554.
- [6] Cliffe M.J., Dove M.T., Drabold D.A., Goodwin A.L. Structure determination of disordered materials from diffraction data. *Physical Review Letters*. 2010;104(12):125501.
- [7] Meyer J.C., Girit C.O., Crommie M.F., Zettl A. Imaging and dynamics of light atoms and molecules on graphene. *Nature*. 2008;454(7202):319–322.
- [8] Zheng Z., Wang F., Han Y. Glass transitions in quasi-two-dimensional suspensions of colloidal ellipsoids. *Physical Review Letters*. 2011;107(6):065702.
- [9] Huang P.Y., Kurasch S., Srivastava A., Skakalova V., Kotakoski J., Krasheninnikov A.V., et al. Direct imaging of a two-dimensional silica glass on graphene. *Nano Letters*. 2012;12(2):1081–1086.
- [10] Lichtenstein L., Heyde M., Freund H.-J. Crystalline-vitreous interface in two dimensional silica. *Physical Review Letters*. 2012;109(10):106101.
- [11] Bernal J.D. A geometrical approach to the structure of liquids. *Nature*. 1959;183(4655):141–147.
- [12] Gaskell P.H. A new structural model for transition metal–metalloid glasses. *Nature*. 1978;276(5687):484–485.
- [13] Levine D., Steinhardt P.J. Quasicrystals: a new class of ordered structures. *Physical Review Letters*. 1984;53(26):2477.
- [14] Huang P.Y., Ruiz-Vargas C.S., van der Zande A.M., Whitney W.S., Levendorf M.P., Kevek J.W., et al. Grains and grain boundaries in single-layer graphene atomic patchwork quilts. *Nature*. 2011;469(7330):389–392.
- [15] Löffler D., Uhrich J.J., Baron M., Yang B., Yu X., Lichtenstein L., et al. Growth and structure of crystalline silica sheet on Ru (0001). *Physical Review Letters*. 2010;105(14):146104.
- [16] Yu X., Yang B., Boscoboinik J.A., Shaikhutdinov S., Freund H.-J. Support effects on the atomic structure of ultrathin silica films on metals. *Applied Physics Letters*. 2012;100(15):151608.
- [17] Wu W., Zhang L., Ren H., Zhang K., Li H., He Y. Synergy and pinning effects in a monatomic liquid film in confined conditions. *Physical Chemistry Chemical Physics*. 2015;17(20):13380–13386.

- [18] Zhang K., Jiang Y.Y., Li H., Si P.C., Li Y.F., Yu H.Q. Power-law scaling of dynamical and structural signatures in liquid metallic nano-film. *Europhysics Letters*. 2011;96(4):46005.
- [19] Zhang K., Li H., Li L., Bian X.F. Why does the second peak of pair correlation functions split in quasi-two-dimensional disordered films?. *Applied Physics Letters*. 2013;102(7):071907.
- [20] Zhou X.W., Wadley H.N.G., Johnson R.A., Larson D.J., Tabat N., Cerezo A. Atomic scale structure of sputtered metal multilayers. *Acta Materialia*. 2001;49(19):4005–4015.
- [21] Plimpton S. Fast parallel algorithms for short-range molecular dynamics. *Journal of Computational Physics*. 1995;117(1):1–19.
- [22] Nosé S. A unified formulation of the constant temperature molecular dynamics methods. *Journal of Chemical Physics*. 1984;81(1):511–519.
- [23] Berardi C.R., Barros K., Douglas J.F., Losert W. Direct observation of stringlike collective motion in a two-dimensional driven granular fluid. *Physical Review E*. 2010;81(4):041301.
- [24] Donati C., Douglas J.F., Kob W., Plimpton S.J., Poole P.H., Glotzer S.C. Stringlike cooperative motion in a supercooled liquid. *Physical Review Letters*. 1998;80(11):2338.
- [25] Gebremichael Y., Vogel M., Glotzer S.C. Particle dynamics and the development of string-like motion in a simulated monoatomic supercooled liquid. *Journal of Chemical Physics*. 2004;120(9):4415–4427.
- [26] Elliott S.R. Medium-range structural order in covalent amorphous solids. *Nature*. 1991;354(354):445–452.
- [27] Morozov I.V., Kazennov A.M., Bystryi R.G., Norman G.E., Pisarev V.V., Stegailov V.V. Molecular dynamics simulations of the relaxation processes in the condensed matter on GPUs. *Computer Physics Communications*. 2011;182(9):1974–1978.
- [28] Cleveland C.L., Luedtke W.D., Landman U. Melting of gold clusters: icosahedral precursors. *Physical Review Letters*. 1998;81(10):2036.
- [29] Tsuzuki H., Branicio P.S., Rino J.P. Structural characterization of deformed crystals by analysis of common atomic neighborhood. *Computer Physics Communications*. 2007;177(6):518–523.
- [30] Liu X.J., Xu Y., Hui X., Lu Z.P., Li F., Chen G.L., et al. Metallic liquids and glasses: atomic order and global packing. *Physical Review Letters*. 2010;105(15):155501.
- [31] Truskett T.M., Torquato S., Sastry S., Debenedetti P.G., Stillinger F.H. Structural precursor to freezing in the hard-disk and hard-sphere systems. *Physical Review E*. 1998;58(3):3083.

- [32] Faken D., Jónsson H. Systematic analysis of local atomic structure combined with 3D computer graphics. *Computational Materials Science*. 1994;2(2):279–286.
- [33] Honeycutt J.D., Andersen H.C. Molecular dynamics study of melting and freezing of small Lennard-Jones clusters. *Journal of Physical Chemistry*. 1987;91(19):4950–4963.
- [34] Candelier R., Dauchot O., Biroli G. Building blocks of dynamical heterogeneities in dense granular media. *Physical Review Letters*. 2009;102(8):088001.
- [35] Garrahan J.P., Chandler D. Geometrical explanation and scaling of dynamical heterogeneities in glass forming systems. *Physical Review Letters*. 2002;89(3):035704.
- [36] Widmer-Cooper A., Harrowell P. Predicting the long-time dynamic heterogeneity in a supercooled liquid on the basis of short-time heterogeneities. *Physical Review Letters*. 2006;96(18):185701.
- [37] Mizuno H., Yamamoto R. Lifetime of dynamical heterogeneity in a highly supercooled liquid. *Physical Review E*. 2010;82(3):030501.
- [38] Schöpe H.J., Bryant G., van Meegen W. Two-step crystallization kinetics in colloidal hard-sphere systems. *Physical Review Letters*. 2006;96(17):175701.
- [39] Ten Wolde P.R., Ruiz-Montero M.J., Frenkel D. Numerical evidence for bcc ordering at the surface of a critical fcc nucleus. *Physical Review Letters*. 1995;75(14):2714.
- [40] Kelton K.F., Lee G.W., Gangopadhyay A.K., Hyers R.W., Rathz T.J., Rogers J.R., et al. First X-ray scattering studies on electrostatically levitated metallic liquids: demonstrated influence of local icosahedral order on the nucleation barrier. *Physical Review Letters*. 2003;90(19):195504.
- [41] Kobayashi K., Salam M.U. Comparing simulated and measured values using mean squared deviation and its components. *Agronomy Journal*. 2000;92(2):345–352.
- [42] Bennett C.H. Serially deposited amorphous aggregates of hard spheres. *Journal of Applied Physics*. 1972;43(6):2727–2734.
- [43] Ma D., Stoica A.D., Wang X.-L. Power-law scaling and fractal nature of medium-range order in metallic glasses. *Nature Materials*. 2009;8(1):30–34.

